European Journal of Pharmaceutics and Biopharmaceutics 184 (2023) 116–124

Contents lists available at ScienceDirect

European Journal of Pharmaceutics and Biopharmaceutics

journal homepage: www.elsevier.com/locate/ejpb

Research paper

Plasma membrane depolarization reveals endosomal escape incapacity of cell-penetrating peptides

Marc Serulla [a], Palapuravan Anees [b,c], Ali Hallaj [a], Evgeniya Trofimenko [a], Tara Kalia [b], Yamuna Krishnan [b,c], Christian Widmann [a,*]

[a] Department of Biomedical Sciences, University of Lausanne, 1005 Lausanne, Switzerland
[b] Department of Chemistry, The University of Chicago, Chicago, IL 60637, USA
[c] Grossman Institute of Neuroscience, Quantitative Biology and Human Behavior, The University of Chicago, Chicago, IL 60637, USA

ARTICLE INFO

Keywords:
Cell-penetrating peptides
Endosomal escape
Direct translocation
Plasma membrane potential
Endosomes
LLOME

ABSTRACT

Cell-penetrating peptides (CPPs) are short (<30 amino acids), generally cationic, peptides that deliver diverse cargos into cells. CPPs access the cytosol either by direct translocation through the plasma membrane or via endocytosis followed by endosomal escape. Both direct translocation and endosomal escape can occur simultaneously, making it non-trivial to specifically study endosomal escape alone. Here we depolarize the plasma membrane and showed that it inhibits the direct translocation of several CPPs but does not affect their uptake into endosomes. Despite good endocytic uptake many CPPs previously considered to access the cytosol via endosomal escape, failed to access the cytosol once direct translocation was abrogated. Even CPPs designed for enhanced endosomal escape actually showed negligible endosomal escape into the cytosol. Our data reveal that cytosolic localization of CPPs occurs mainly by direct translocation across the plasma membrane. Cell depolarization represents a simple manipulation to stringently test the endosomal escape capacity of CPPs.

1. Introduction

Cell-penetrating peptides (also called cell-permeable peptides) are short (<30 amino acids), generally cationic, peptides that can enter cells. CPPs facilitate the cellular entry of diverse payloads that are hooked onto them for diagnostic and therapeutic purposes [1,2]. CPPs enter cells both by endocytosis and by direct translocation across the plasma membrane. We and others have shown that very low membrane potentials trigger the formation of transient water pores of ~ 2 nm in diameter that CPPs exploit to move into the cytosol via a process called direct translocation [3–7]. Depolarizing the plasma membrane, genetically or pharmacologically, prevents such direct translocation [3].

CPPs can also enter cells via endocytic uptake, which is unaffected by the plasma membrane potential [3,8]. To access the cytosol post-endocytosis, CPPs must be able to exit the compartment by a process called endosomal escape [9–12]. Endosomal escape is poorly understood at the molecular level since direct translocation and endosomal escape of CPPs occur simultaneously. Therefore, it is extremely challenging to specifically evaluate the fraction of cytosolic CPPs that arises exclusively from endosomal escape. Consequently, the endosomal escape of CPPs as a route to cytosolic access remains vigorously debated. Several studies have suggested endosomal escape as the sole pathway by which CPPs access the cytosol. However the contribution of direct translocation for CPP cytosolic access was largely unaddressed in these studies [13–18]. Importantly, recent work indicates that endocytosed CPPs remain trapped in endosomes, raising the possibility that endosomal escape may not be the dominant route by which CPPs access the cell's cytosol [3,19–23].

Here, we show that depolarizing the plasma membrane effectively inhibits CPP direct translocation without affecting CPP endosomal uptake. By depolarizing cells, we could therefore precisely evaluate the endosomal escape capacities of R9 and TAT, two of the most widely used CPPs in biology and medicine, as well as a series of CPPs that have been designed to enhance their endosomal escape properties. We also tested the endosomal escape capacity of a TAT-bound peptidic cargo and of the homeodomain (HD) of OTX2 that naturally contains CPP-like sequences. Our results indicate that CPP cytosolic acquisition occurs predominantly, if not exclusively, through direct translocation.

* Corresponding author at: Department biomedical sciences, Rue du Bugnon 7, 1005 Lausanne, Switzerland.
E-mail address: Christian.Widmann@unil.ch (C. Widmann).

https://doi.org/10.1016/j.ejpb.2023.01.019
Received 7 June 2022; Received in revised form 12 December 2022; Accepted 23 January 2023
Available online 26 January 2023

2. Results

We recently showed that plasma membrane hyperpolarization is required for cationic CPPs to directly translocate into the cytosol [3]. We therefore tested whether by depolarizing cells we could block direct translocation of CPPs, without affecting their endocytic uptake. We first tested whether plasma membrane depolarization had any effect on endocytosis or on endosomal membrane potential [24]. After loading the cells with CPPs, we then removed as much extracellular CPPs as possible by rigorous washing including cell trypsinization and reseeding (Figure S1). We then monitored the ability of endocytosed CPPs to access the cytosol over time.

2.1. Plasma membrane depolarization does not affect CPP endocytosis nor endosomal membrane potential

We depolarized cells by incubating them in media containg high potassium concentrations. This medium was made by using an experimental medium lacking sodium and potassium salts that was then supplemented with 100 mM KCl. We named this high potassium concentration medium "depolarization medium". Similarly, we created a control medium containing 5.3 mM KCl (Table S1). A thirty-minute incubation in depolarization medium led to a cell membrane depolarization from −30 mV to −10 mV in HeLa cells (Fig. S2A) without affecting their viability (Fig. S2B). Plasma membrane depolarization did not alter the endocytic uptake of R9, a prototypic cationic CPP (Figure S3) nor did it alter the colocalization of R9-containing puncta with early (EEA1) or late (LAMP1) endosomes as revealed by confocal live cell imaging (Fig. 1 A). We tested whether depolarization impacted the pH of endosomes using either a dextran ratiometric pH sensor (Fig. S4A-B) or a lysosomal pH sensitive dye (LysoSensor Green DND-189) (Fig. S4C). We found that depolarization did not affect endosomal acidification, while bafilomycin A1, a V-ATPase inhibitor, did, as expected (Fig. S4B-C).

We next determined whether the depolarization medium affected the membrane potential of endosomes. To do this, we used an organelle-targetable, DNA-based ratiometric fluorescent-based voltmeter called VoltairIM that labels specific endosomal compartments via hMSR1 human macrophage scavenger receptor-mediated endocytosis [24,25]. A voltage-insensitive version of VoltairIM (ds-Atto647) colocalized with Rab5-positive early endosomes and Rab7-positive late endosomes 30 and 90 min after its addition to HeLa cells, respectively (Figure S5). We therefore used these time points to measure the membrane potential of early and late endosomes using VoltairIM. When cells were depolarized and incubated in depolarization medium, early endosomes were depolarized but late endosomes were not (condition 3 in Fig. 1B). However, when cells were depolarized and then incubated in control medium, both early and late endosomes showed membrane potentials (condition 2 in Fig. 1B) comparable to untreated controls (condition 1 in Fig. 1B). These data indicate that endosome membrane potential is preserved when CPP-loaded endosomes are assayed for endosomal escape.

2.2. The R9 CPP remains in endosomes

To investigate whether plasma membrane depolarization was sufficient to block R9 cytosolic entry, we loaded HeLa cells with increasing concentrations of R9 in depolarization medium (100 mM KCl) and control medium (5.33 mM KCl). Depolarization strongly inhibited R9-TAMRA cytosolic localization but not the formation of CPP-loaded endosomes (Fig. 2A). Image quantitation revealed that cytosolic signal was not detected in cells treated with 1 μM R9 (Fig. 2A, Table S2). Above 1 μM R9, plasma membrane depolarization substantially inhibited cytosolic localization of R9-TAMRA (Fig. 2A and Table S2). This indicates that cell depolarization efficiently inhibits the cytosolic access of CPPs via direct translocation. Depolarization can therefore permit one to precisely address the extent of CPP endosomal escape.

Next, we proceeded to see if endosomes release their CPP content in the cytosol over time (scheme in Fig. 2B). Our assay allows detection of endosomal escape if ~ 5 % of the endosomal CPP content is released in the cytosol when 2 μM of R9 are used to load cells (see the methods). Time course experiments using depolarized cells incubated with 2 μM of R9-TAMRA and then incubated in regular culture medium revealed no increase in R9 cytosolic fluorescence (Fig. 2B and Figure S6). However, when L-leucyl-L-leucine methyl ester hydrobromide (LLOME), a lysosomal leakage-inducing compound [26,27], was added to these cells, endosomal escape was readily observed (Fig. 2B and Figure S7A). Similar results were obtained when R9 was labelled with TF2WS, a fluorophore distinct from TAMRA (Figure S7B). At the concentration used here, LLOME was not toxic to cells (Figure S7C). We also analysed the variation of the cytosolic fluorescence of cells loaded with 2 μM R9-TAMRA as a function of time at the single cell level and found no evidence for endosomal escape (Figure S8). If low enough R9-TAMRA concentrations (≤1 μM) are used, no cytosolic entry from the extracellular milieu is detected and hence plasma membrane depolarization is dispensable in this case (see Fig. 2). In cells loaded with 1 μM R9-TAMRA, we did not detect endosomal escape whether the cells were depolarized or not. In both control and depolarizing conditions, similar cytosolic CPP concentrations were obtained following LLOME addition, indicating that the initial endosomal loading was equivalent (Figure S9).

To evaluate if endosomal escape can be detected at higher CPP concentrations, we exposed depolarized HeLa cells to 5 μM R9-TAMRA. However, we saw no change in CPP fluorescence over the background signal (Figure S10). Only when LLOME was added could we detect an increase in cytosolic levels of R9-TAMRA (Figure S10). Similar results were observed in DLD-1 cells (Figure S11). Endosomal escape may occur rapidly after formation of endosomes but not at later time points. In such a case, as our procedure requires a reseeding step of 60 min, we may have missed the time window of endosomal escape. We therefore assessed whether an increase in cytosolic signal could be detected immediately after the CPP loading and washing steps. Here, we used heparin to strip the cell surface of adhered R9-TAMRA (see Fig. S1A). Even then, no increase in cytosolic signal could be detected (Figure S12). This indicates that endosomal escape of R9-TAMRA does not occur rapidly after its uptake into endosomes. In sum, these results show that R9 endosomal escape does not occur unless it is induced by agents like LLOME that perforate endosomal compartments.

2.3. TAT, another widely used CPP, does not escape endosomes

To test the generality of our findings, we similarly investigated another classical CPP, namely TAT (Fig. 3 and Table S3). The cytosolic entry of TAT-TAMRA was also inhibited by cell depolarization. The inhibition was complete when cells were incubated with ≤ 2 μM of TAT-TAMRA (Fig. 3A and Table S3). No endosomal escape could be detected following the incubation of depolarized HeLa cells with 2 μM of TAT-TAMRA (Fig. 3B). This indicates that, like R9-TAMRA, TAT-TAMRA does not appear to escape endosomes.

2.4. The cytosolic entry pathway of CPPs designed for endosomal escape

Next, we tested a series of CPPs with reported enhanced endosomal escape abilities. TAT dimerization via a disulfide bond generates the dfTAT peptide. The dimerization is considered to enhance endosomal escape [19]. Mechanistically, dfTAT is posited to induce endosomal leakage after interacting with bis(monoacylglycero)phosphate in late endosomes [28]. Here, we used a dfTAT enantiomer (D-dfTAT) that preserves the internalization characteristics of dfTAT but is protease-resistant [29]. Plasma membrane depolarization strongly reduced D-dfTAT levels in the cytosol indicating that direct translocation is the dominant mechanism of CPP entry (Figure S13 and Table S4). However, unlike R9 and TAT, cytosolic D-dfTAT entry could not be fully inhibited by depolarization (Figure S13). Time-course experiments reveal no

increase in cytosolic fluorescence upon loading endosomes with D-dfTAT (Fig. 4 and S14). We ruled out a fast-occurring endosomal escape, by probing for cytosolic signal in non-trypsinized cells (Figure S15). Additionally, we did not observe endosomal escape in non-depolarized cells loaded with a low concentration (1 μM) of D-dfTAT (Figure S16). Overall, this data indicates that the main mode of D-dfTAT cytosolic entry is direct translocation and not endosomal escape. Next, we considered cyclic arginine-rich peptides that have been reported to

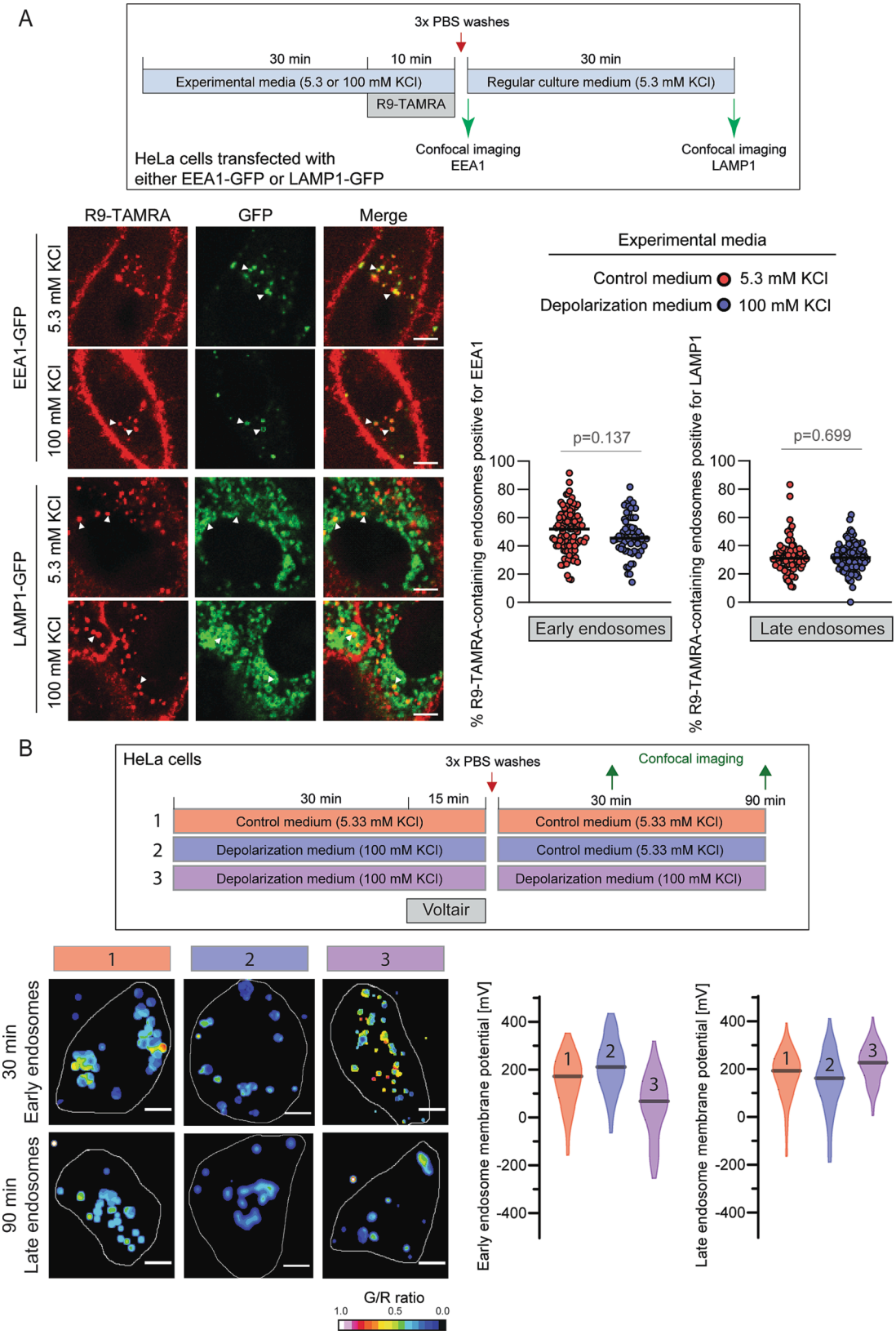

(caption on next page)

Fig. 1. Plasma membrane depolarization does not affect CPP endocytosis nor the membrane potential of endosomes. The experimental conditions are depicted schematically above the data. **A**. One hundred thousand HeLa cells were seeded per condition. Cells were transfected with plasmids expressing EEA1-GFP (early endosomes) or LAMP1-GFP (late endosomes) endocytic markers. Forty-eight hours later, cells were switched to experimental RPMI 1640 containing 5.3 or 100 mM KCl for 30 min and incubated with 2 μM of R9-TAMRA for 10 min. Cells were PBS-washed three times. Fresh regular RPMI 1640 culture media was then added. Cells expressing EEA1 were immediately imaged by confocal microscopy while cells expressing LAMP1 were imaged after a 30 min incubation period at 37 °C. TAMRA and GFP colocalization was quantitated as previously described [8]. Each dot in the graphs represents the percentage, for a given cell, of the R9-TAMRA-containing endosomes positive for the indicated markers. Statistical analysis: unpaired t-tests. Representative images (scale bar: 5 m) of each condition are shown. Arrows point to colocalization between R9-TAMRA and the indicated GFP-labelled endocytic markers. **B** Representative pseudo-colored G/R ratio images of the Voltair-labelled endosomes (the G/R ratio is explained in the methods). Scale bar = 10 μm. The quantitation of the membrane potentials of early and late endosomes in cells subjected to the indicated experimental conditions is shown as violin plots on the right-hand side of the figure. The grey bars represent the median. Al least 100 vesicles were analyzed per condition.

improve cytosolic access compared to arginine-rich linear CPPs like TAT and R9 [17,18]. In this class, CPP12 is one of the most efficient CPPs [17]. As observed with D-dfTAT, we were unable to detect endosomal escape of CPP12 when it was loaded in endosomes (Fig.s 4, S17, S18, S19 and Table S5). Finally, certain small proteins containing a discrete array of five arginines on a folded α-helix, such as ZF5.3, have been considered to show enhanced endosomal escape [15,16]. Contrary to the peptides so far studied, ZF5.3 did not show much cytosolic localization at ≤ 5 μM (Figure S20 and Table S6). Above 5 μM, cytosolic signal was observed that was partially lost when cells were depolarized. This indicates that at least a fraction of cytosolic entry occurs via direct translocation (Figure S20 and Table S6). Once ZF5.3 was loaded in endosomes followed by washing, no further cytosolic signal increase was seen, unless induced by LLOME (Fig. 4). The heparin wash was not as effective to remove surface bound ZF5.3 unlike the other CPPs (Figure S21). The mode of plasma membrane interaction of ZF5.3 versus CPPs such as R9 and TAT appears therefore to differ.

2.5. CPPs hooked to cargos and homeodomains remain trapped in endosomes.

We next determined if the addition of a cargo to a CPP affects its endosomal escape capacity. For this purpose, we used the TAT-RasGAP$_{317-326}$ anticancer and antimicrobial peptide [3,4,30–38]. This compound is made of the TAT CPP and the 317–326 sequence of p120 RasGAP. As was the case for the unhooked TAT, depolarization drastically reduced TAT-RasGAP$_{317-326}$ cytosolic uptake. Time course experiment did not reveal TAT-RasGAP$_{317-326}$ endosomal escape unless the endosmolytic agent LLOME was added (Figure S22 and Table S7).

We also tested the endosomal escape capacity of the OTX2 HD [39]. HDs are present in homeoproteins, a family of transcription factors involved in tissue patterning, axon guidance, cell migration during development, and neuroplasticity [40–43]. Homeoproteins can cross biological membranes thanks to the CPP-like sequences in their HD [40,42,44–48]. Plasma membrane depolarization reduced OTX2 HD cytosolic staining and in this condition no cytosolic acquisition could be evidenced over time (Figure S23 and Table S8).

2.6. Energy depletion blocks CPP direct translocation and endocytosis

Contrary to endocytosis, direct translocation of CPPs is sometimes considered an energy-independent process [1,2,10]. Hence, some earlier studies used energy depletion to block endocytosis with the assumption that direct translocation remained active and therefore amenable to investigation [49–52]. We and others have shown that adequate plasma membrane hyperpolarization is required for direct translocation of CPPs [3–7]. Membrane potential maintenance requires the activity of the ATP-dependent sodium potassium pump [53]. Nevertheless, we sought to test whether direct translocation was energy independent. We used metabolic inhibitors (NaN_3 and 2-deoxy-D-glucose) in culture media without glucose, [54] to decrease ATP levels and depolarize the plasma membrane in HeLa cells (Figure S24A-B). Under these conditions, we incubated HeLa cells with a concentration of R9-TAMRA (2 μM) that favors endocytic uptake or with a concentration of the peptide (10 μM) that permits direct translocation as well as endocytic uptake. Figure S24C shows that the metabolic inhibitors completely abolished R9-TAMRA uptake into both cytosol and into endosomes. This demonstrates that both CPP endocytosis and direct translocation are energy-dependent and thus that energy depletion cannot discriminate between either mechanism.

3. Discussion

CPPs can enter cells by direct translocation through the plasma membrane as well as via endocytosis [3]. Endocytosed CPPs may then escape into the cytosol. Conceptually, both direct translocation and endosomal escape can contribute to the cytosolic entry of CPPs. To study endosomal escape, it is essential to rule out entry via direct translocation. Here, we present a simple method to distinguish endosomal escape from direct translocation that only requires the use of labelled CPPs, potassium-rich media, and confocal imaging.

Potassium-rich media depolarize cells, efficiently inhibiting direct translocation yet permitting endocytosis of CPPs. Our assay is reasonably sensitive as we can detect endosomal escape at low micromolar CPP concentrations (~0.5 μM) and when only < 5 % of the endosomal content is released in the cytosol (see methods). We found that the dominant mode of cytosolic entry of R9, TAT, D-dfTAT, CPP12, ZF5.3 was via direct translocation and that endosomal escape was negligible.

Previously, endocytic inhibitors [16,55–57] and ATP depletion [49–52,57–59] were used to distinguish direct translocation from endosomal escape. We have recently demonstrated that CPPs are endocytosed via a pathway that is different from clathrin-mediated endocytosis or macropinocytosis [8]. Indeed, maturation of CPP-containing endosomes to LAMP1-positive vesicles requires Rab14 but not Rab5 or Rab7. Formation of CPP-containing vesicles is insensitive to inhibitors (e.g. PI3K inhibitors, dynamin dominant negative mutants, and macropinosome formation inhibitors) that prevent classical endocytosis [8]. Thus, these inhibitors cannot be used to investigate how CPPs enter cells.

A recent sophisticated technique using split luciferase escape quantitation (SLEEQ) has been used by Teo and collaborators to investigate CPP endosomal escape [23]. This approach is based on two Nanoluciferase fragments: the 11 amino acid HiBit peptide and a larger LgBit fragment. HiBit and LgBit can bind each other with high affinity and recreate a functional luciferase enzyme. CPPs were hooked to Hibit and LgBit was expressed in the cell's cytosol. If CPPs escape endosomes, the nanoluciferase enzyme is reconstituted in the cytosol and this allows light production upon fumarizine addition. Such assays are extremely sensitive and while they can detect minimal endosomal escape, they lack spatial resolution and require genetic modification of the cellular system [15,60–62]. Even by these methods, CPPs were shown to have a limited endosomal escape capacity, i.e., ≤7% in HeLa cells and ≤ 2 % in HeK293T cells.

Here we demonstrate a simple approach to study endosomal escape of CPPs without the confounding effect of direct translocation. However, our strategy has a few limitations. Although it provides good spatial resolution, it is not as sensitive as the signal amplifying methods described above. We rely on time to monitor endosomal escape. This

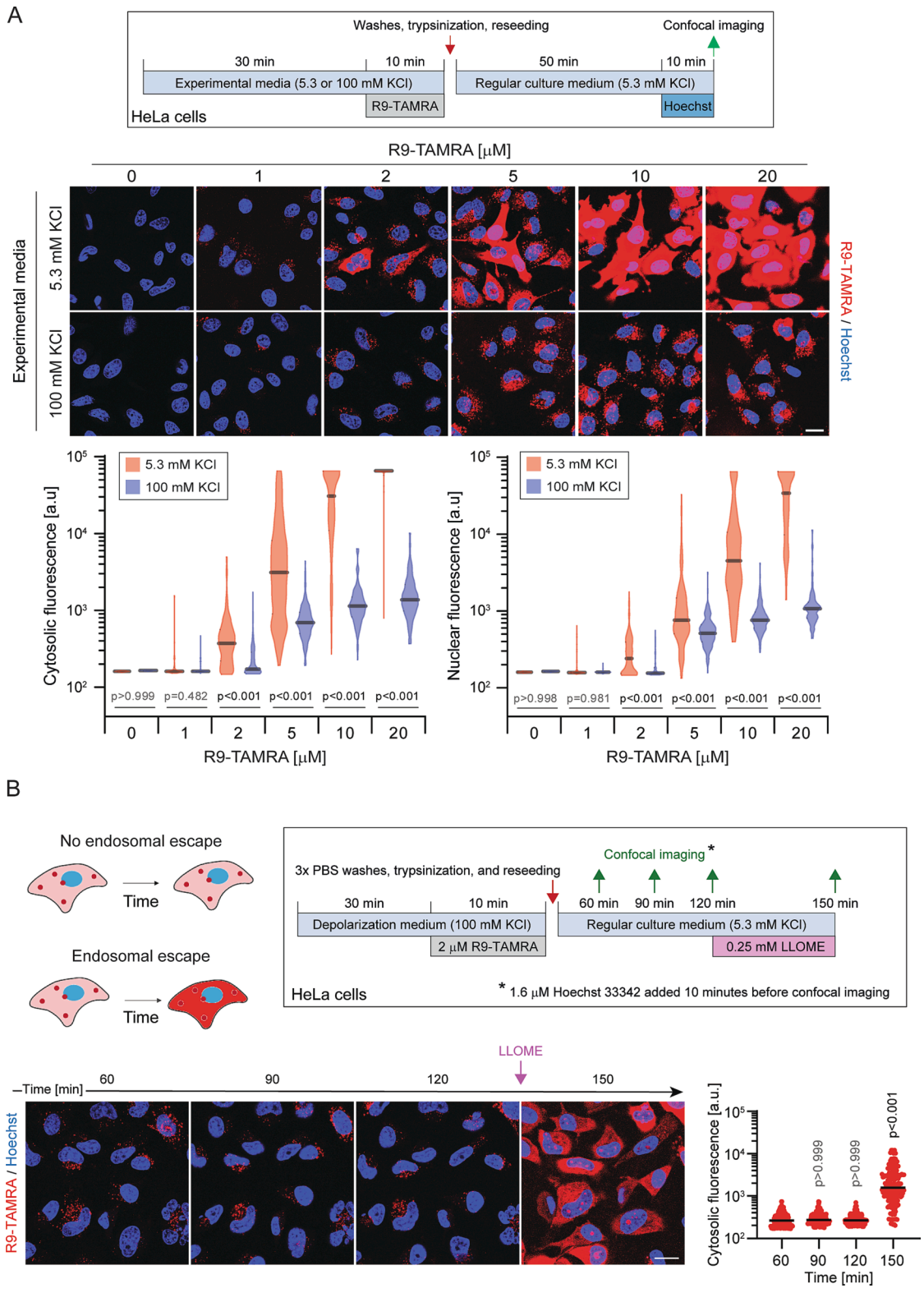

Fig. 2. No evidence for R9 endosomal escape. **A**. Hela cells were subjected to the experimental conditions depicted schematically at the top of the panel (see the methods for details). Representative images (scale bar: 20 μm) from two independent experiments are shown. Image analysis was performed with automated analysis except for the 5, 10, and 20 μM of R9-TAMRA conditions in 5.3 mM KCl culture medium that were quantitated manually. Grey bars represent the median. Data were transformed to log10(x) prior to two-way ANOVAs with Sidak's post-hoc test to generate the p values for the indicated comparisons. Statistical assessment of the difference between a given condition and the "0 μM R9-TAMRA" condition is presented in Table S1. **B**. Top left: Representation of the possible scenarios after endosomes are loaded with a TAMRA labelled CPP. Top right: The experimental conditions are depicted schematically in the inset. Below part: Representative images (scale bar: 20 μm) from two independent experiments are shown. Quantitation was performed with the automated procedure described in the methods except for the conditions with 0.25 mM of LLOME that were manually quantitated. Each dot represents an individual cell and black bars correspond to medians. For statistical analysis, data were transformed to log10(x) prior to performing one-way ANOVA tests with Dunnett's post-hoc test against the "time 60" condition.

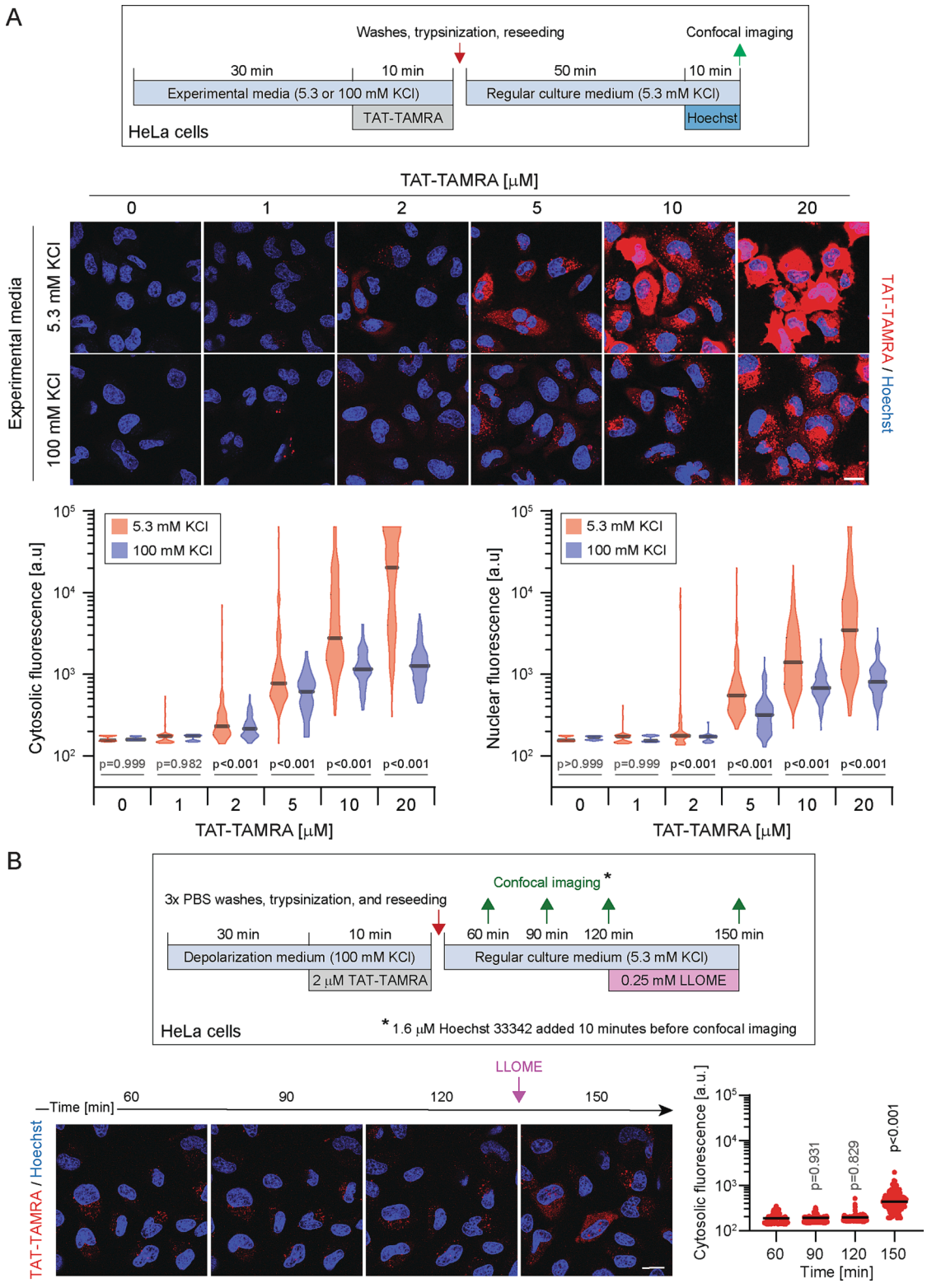

Fig. 3. TAT does not escape endosomes. A. The experimental conditions are depicted schematically above the data. Representative images (scale bar: 20 μm) from two independent experiments are shown. Quantitation was performed with the automated procedure described in the methods except for the 10 and 20 μM TAT-TAMRA conditions in the presence of 5.3 mM of KCl that were quantitated manually. Grey bar represents the median. For statistical analyses of the indicated conditions, data were transformed to log10(x) prior to two-way ANOVAs followed with Sidak's post-hoc test. The comparison with the "0 μM TAT-TAMRA" condition is presented in Table S3. **B.** The experimental conditions are depicted schematically above the data. Representative images (scale bar: 20 μm) from two independent experiments are shown. Quantitation was performed with the automated procedure described in the methods except for the conditions with 0.25 mM of LLOME that were manually quantitated. Each dot represents an individual cell and black bars correspond to the median. For statistical analyses, data were transformed to log10 (x) prior to applying one-way ANOVAs with Dunnett's post-hoc tests against the "60 min" condition.

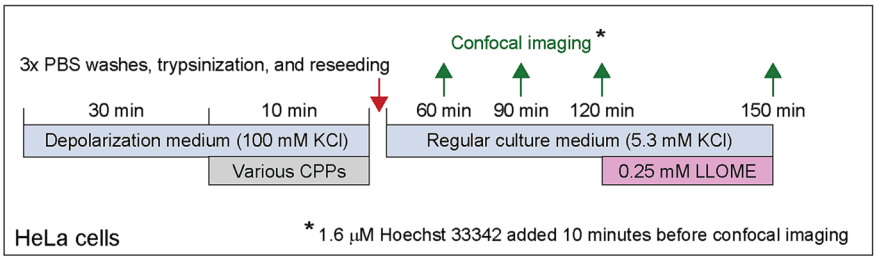

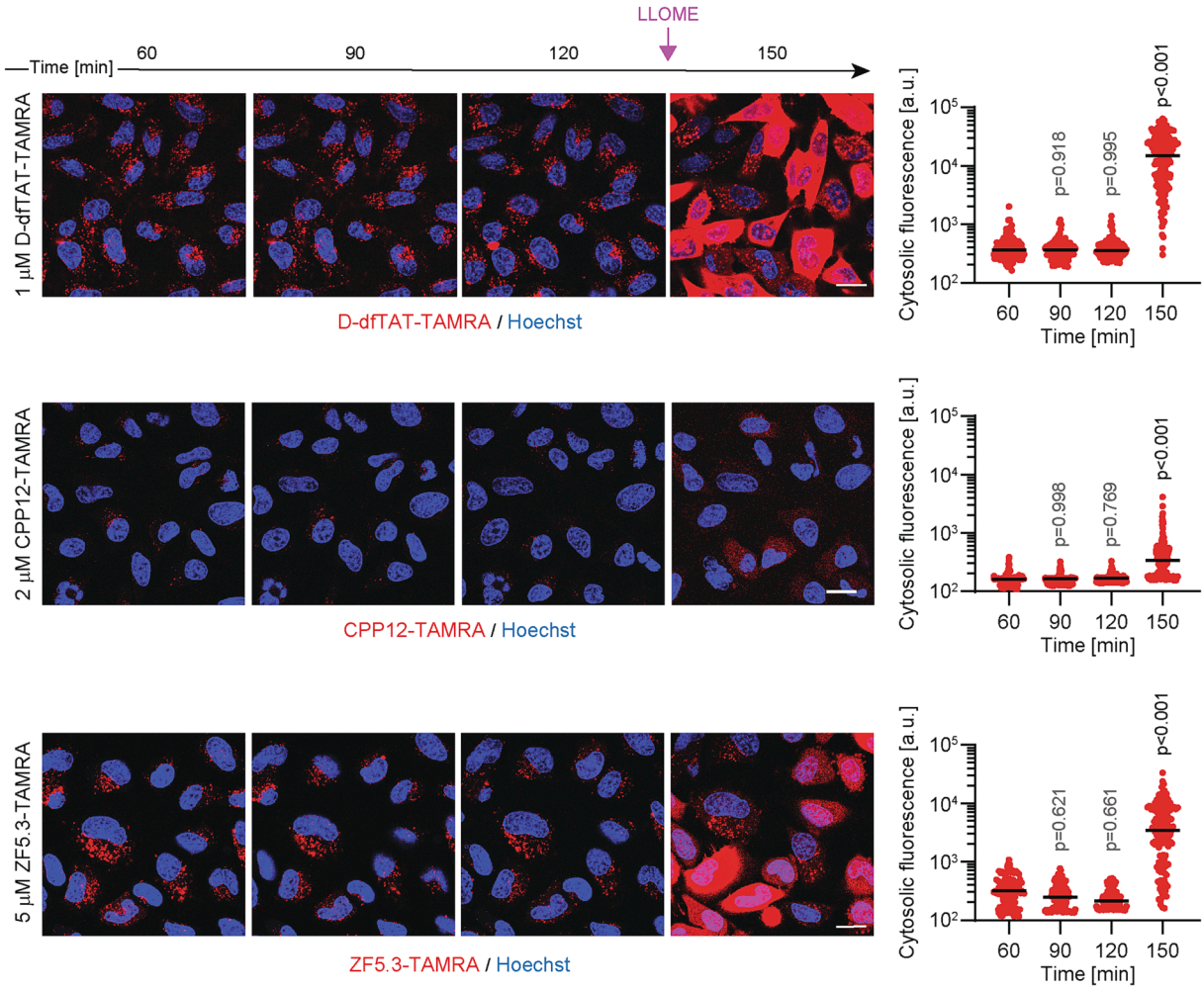

Fig. 4. Evaluation of the endosomal escape capacity of D-dfTAT, CPP12, and ZF5.3. The experimental conditions are depicted schematically above the data. Representative images (scale bar: 20 μm) from two independent experiments are shown. Quantitation was performed with the automated procedure described in the methods except for the conditions with 0.25 mM of LLOME that were quantitated manually. Each dot represents an individual cell and black bars correspond to the median. For statistical comparison to the "60 min" condition, data were transformed to log10(x) prior to two-way ANOVAs followed with Dunnett's post-hoc test.

might be problematic for CPPs made of L-amino-acids that can potentially be degraded in cells over time. It is therefore advisable to use CPPs made of D-amino acids when studying CPP uptake, which is what was done for most of the CPPs tested in the present work (Table S9). Our approach requires laser illumination to track CPPs and thus care should be taken to minimize phototoxicity, such as using low intensity lasers [3]. It also has to be taken into consideration that fluorescent dyes linked to CPPs might affect their behavior, including their ability to bind lipids [63,64] and that this might impact negatively on their potential endosomal escape capacity [65]. Finally, we have shown that plasma membrane depolarization does not affect the membrane potential of endosomes containing the hMSR1 human macrophage scavenger receptor that brings the Voltair sensor into cells (see the methods and Fig. 1) [8,24]. We have assumed, but not demonstrated, that this is also the case for CPP-containing endosomes.

In the present work, we have tested in 2D cultures two of the most common CPPs, R9 and TAT, as well as three CPPs designed for endosomal escape. For these, we found very limited, if any, endosomal escape capacities. There are many other CPPs however, and further work is required to determine if they too poorly escape endosomes. Additionally, the role of complex cargos carried by CPPs was not tested here. Complex cargo, such as metal–organic frameworks, could significantly alter the CPP properties [66] and this might impact their endosomal escape property. We also have not evaluated if our depolarization

approach can function in 3D cultures or in tissues.

In conclusion, our study highlights the importance of deconvoluting the contribution of direct translocation and endosomal escape when investigating CPP cytosolic acquisition. Our methodological approach based on cell depolarization allows easy testing of the endosomal escape capacity of CPPs without the need to rely on complex techniques or genetically engineered cell lines.

Declaration of Competing Interest

The authors declare that they have no known competing financial interests or personal relationships that could have appeared to influence the work reported in this paper.

Data availability

Data will be made available on request.

Acknowledgements

We thank Luigi Bozzo and the Cellular Imaging Facility of the University of Lausanne for their support in image acquisition and help with the automated image analysis. This work was supported by FA9550-19-0003 from AFOSR (YK), NIH grants 1R01NS112139-01A1 (YK), the Ono Pharma Foundation Breakthrough Science Award (YK) and the Swiss National Science Foundation (grant 310030_207464 to CW).

Appendix A. Supplementary material

Supplementary data to this article can be found online at https://doi.org/10.1016/j.ejpb.2023.01.019.

References

[1] C. Bechara, S. Sagan, Cell-penetrating peptides: 20 years later, where do we stand? FEBS Lett. 587 (12) (2013) 1693–1702.
[2] G. Guidotti, L. Brambilla, D. Rossi, Cell-penetrating peptides: from basic research to clinics, Trends Pharmacol. Sci. 38 (4) (2017) 406–424.
[3] E. Trofimenko, et al., Genetic, cellular and structural characterization of the membrane potential-dependent cell-penetrating peptide translocation pore, Elife 10 (2021), 2020.02.25.963017.
[4] M. Serulla, et al., TAT-RasGAP$_{317-326}$ kills cells by targeting inner-leaflet-enriched phospholipids, PNAS 117 (50) (2020) 31871–31881.
[5] X. Gao, et al., Membrane potential drives direct translocation of cell-penetrating peptides, Nanoscale 11 (4) (2019) 1949–1958.
[6] M.M.R. Moghal, et al., Role of membrane potential on entry of cell-penetrating peptide Transportan 10 into single vesicles, Biophys. J. 118 (1) (2020) 57–69.
[7] J.B. Rothbard, et al., Role of membrane potential and hydrogen bonding in the mechanism of translocation of guanidinium-rich peptides into cells, J. Am. Chem. Soc. 126 (31) (2004) 9506–9507.
[8] E. Trofimenko, et al., The endocytic pathway taken by cationic substances requires Rab14 but not Rab5 and Rab7, Cell Rep. 37 (5) (2021), 109945.
[9] J. Allen, et al., Cytosolic delivery of macromolecules in live human cells using the combined endosomal escape activities of a small molecule and cell penetrating peptides, ACS Chem. Biol. (2019).
[10] J.C. LeCher, S.J. Nowak, J.L. McMurry, Breaking in and busting out: cell-penetrating peptides and the endosomal escape problem, Biomol. Concepts 8 (3–4) (2017) 131–141.
[11] D. Pei, M. Buyanova, Overcoming endosomal entrapment in drug delivery, Bioconjug. Chem. 30 (2) (2019) 273–283.
[12] A. El-Sayed, S. Futaki, H. Harashima, Delivery of macromolecules using arginine-rich cell-penetrating peptides: ways to overcome endosomal entrapment, AAPS J. 11 (1) (2009) 13–22.
[13] S.M. Fuchs, R.T. Raines, Pathway for polyarginine entry into mammalian cells, Biochemistry 43 (9) (2004) 2438–2444.
[14] G. Drin, et al., Studies on the internalization mechanism of cationic cell-penetrating peptides, J. Biol. Chem. 278 (33) (2003) 31192–31201.
[15] A. Steinauer, et al., HOPS-dependent endosomal fusion required for efficient cytosolic delivery of therapeutic peptides and small proteins, Proc. Natl. Acad. Sci. 116 (2) (2019) 512–521.
[16] J.S. Appelbaum, et al., Arginine topology controls escape of minimally cationic proteins from early endosomes to the cytoplasm, Chem. Biol. 19 (7) (2012) 819–830.
[17] Z. Qian, et al., Discovery and mechanism of highly efficient cyclic cell-penetrating peptides, Biochemistry 55 (18) (2016) 2601–2612.
[18] A. Sahni, Z. Qian, D. Pei, Cell-penetrating peptides escape the endosome by inducing vesicle budding and collapse, ACS Chem. Biol. 15 (9) (2020) 2485–2492.
[19] A. Erazo-Oliveras, et al., Protein delivery into live cells by incubation with an endosomolytic agent, Nat. Methods 11 (2014) 861.
[20] C.S. Breton, et al., Combinative effects of beta-Lapachone and APO866 on pancreatic cancer cell death through reactive oxygen species production and PARP-1 activation, Biochimie 116 (2015) 141–153.
[21] Y.-J. Lee, S. Datta, J.-P. Pellois, Real-time fluorescence detection of protein transduction into live cells, J. Am. Chem. Soc. 130 (8) (2008) 2398–2399.
[22] Y.-J. Lee, et al., A HA2-Fusion tag limits the endosomal release of its protein cargo despite causing endosomal lysis, Biochim. Biophys. Acta Gen. Subj. 1810 (8) (2011) 752–758.
[23] S.L.Y. Teo, et al., Unravelling cytosolic delivery of cell penetrating peptides with a quantitative endosomal escape assay, Nat. Commun. 12 (1) (2021) 3721.
[24] A. Saminathan, et al., A DNA-based voltmeter for organelles, Nat. Nanotechnol. 16 (1) (2021) 96–103.
[25] S. Modi, et al., Two DNA nanomachines map pH changes along intersecting endocytic pathways inside the same cell, Nat. Nanotechnol. 8 (6) (2013) 459–467.
[26] I. Maejima, et al., Autophagy sequesters damaged lysosomes to control lysosomal biogenesis and kidney injury, EMBO J. 32 (17) (2013) 2336–2347.
[27] U. Repnik, et al., L-leucyl-L-leucine methyl ester does not release cysteine cathepsins to the cytosol but inactivates them in transiently permeabilized lysosomes, J. Cell Sci. 130 (18) (2017) 3124–3140.
[28] A. Erazo-Oliveras, et al., The late endosome and its lipid BMP act as gateways for efficient cytosolic access of the delivery agent dfTAT and its macromolecular cargos, Cell Chem. Biol. 23 (5) (2016) 598–607.
[29] K. Najjar, et al., An l- to d-amino acid conversion in an endosomolytic analog of the cell-penetrating peptide TAT influences proteolytic stability, endocytic uptake, and endosomal escape, J. Biol. Chem. 292 (3) (2017) 847–861.
[30] D. Michod, et al., Effect of RasGAP N2 fragment-derived peptide on tumor growth in mice, J. Natl Cancer Inst. 101 (11) (2009) 828–832.
[31] D. Michod, et al., A RasGAP-derived cell permeable peptide potently enhances genotoxin-induced cytotoxicity in tumor cells, Oncogene 23 (55) (2004) 8971–8978.
[32] D. Barras, et al., A WXW motif is required for the anticancer activity of the TAT-RasGAP317-326 peptide, J. Biol. Chem. 289 (34) (2014) 23701–23711.
[33] D. Barras, et al., Fragment N2, a caspase-3-generated RasGAP fragment, inhibits breast cancer metastatic progression, Int. J. Cancer 135 (1) (2014) 242–247.
[34] D. Barras, et al., Inhibition of cell migration and invasion mediated by the TAT-RasGAP317-326 peptide requires the DLC1 tumor suppressor, Oncogene 33 (44) (2014) 5163–5172.
[35] Heulot, M., et al., The TAT-RasGAP 317-326 anti-cancer peptide can kill in a caspase-, apoptosis-, and necroptosis-independent manner. Oncotarget; Vol 7, No 39, 2016.
[36] M. Heulot, et al., The anticancer peptide TAT-RasGAP$_{317-326}$ exerts broad antimicrobial activity, Front. Microbiol. 8 (2017) 994.
[37] M. Georgieva, et al., Bacterial surface properties influence the activity of the TAT-RasGAP$_{317-326}$ antimicrobial peptide, iScience 24 (8) (2021), 102923.
[38] E. Trofimenko, et al., Genetic, cellular, and structural characterization of the membrane potential-dependent cell-penetrating peptide translocation pore, Elife 10 (2021) e69832.
[39] M. Vojtek, et al., Differential repression of Otx2 underlies the capacity of NANOG and ESRRB to induce germline entry, Stem Cell Rep. 17 (1) (2022) 35–42.
[40] A.A. Di Nardo, et al., The physiology of homeoprotein transduction, Physiol. Rev. 98 (4) (2018) 1943–1982.
[41] A. Prochiantz, A.A. Di Nardo, Homeoprotein signaling in the developing and adult nervous system, Neuron 85 (5) (2015) 911–925.
[42] J. Spatazza, et al., Homeoprotein signaling in development, health, and disease: a shaking of dogmas offers challenges and promises from bench to bed, Pharmacol. Rev. 65 (1) (2013) 90–104.
[43] S. Sagan, et al., Homeoproteins and homeoprotein-derived peptides: going in and out, Curr. Pharm. Des. 19 (16) (2013) 2851–2862.
[44] A. Joliot, et al., Antennapedia homeobox peptide regulates neural morphogenesis, Proc. Natl. Acad. Sci. U S A 88 (5) (1991) 1864–1868.
[45] L. Chatelin, et al., Transcription factor hoxa-5 is taken up by cells in culture and conveyed to their nuclei, Mech. Dev. 55 (2) (1996) 111–117.
[46] I. Amblard, et al., Bidirectional transfer of homeoprotein EN2 across the plasma membrane requires PIP2, J. Cell Sci. 133 (13) (2020).
[47] A.H. Joliot, et al., alpha-2,8-Polysialic acid is the neuronal surface receptor of antennapedia homeobox peptide, New Biol.. 3 (11) (1991) 1121–1134.
[48] C.Y. Jiao, et al., Translocation and endocytosis for cell-penetrating peptide internalization, J. Biol. Chem. 284 (49) (2009) 33957–33965.
[49] M. Kosuge, et al., Cellular internalization and distribution of arginine-rich peptides as a function of extracellular peptide concentration, serum, and plasma membrane associated proteoglycans, Bioconjug. Chem. 19 (3) (2008) 656–664.
[50] M.M. Fretz, et al., Temperature-, concentration- and cholesterol-dependent translocation of L- and D-octa-arginine across the plasma and nuclear membrane of CD34+ leukaemia cells, Biochem. J. 403 (2) (2007) 335–342.
[51] C. Allolio, et al., Arginine-rich cell-penetrating peptides induce membrane multilamellarity and subsequently enter via formation of a fusion pore, Proc. Natl. Acad. Sci. U S A 115 (47) (2018) 11923–11928.
[52] H. Hirose, et al., Transient focal membrane deformation induced by arginine-rich peptides leads to their direct penetration into cells, Mol. Ther 20 (5) (2012) 984–993.
[53] J. Bejček, et al., Na^+/K^+-ATPase revisited: on its mechanism of action, role in cancer, and activity modulation, Molecules 26 (7) (2021).

[54] K. Sato, et al., Effects of endocytosis inhibitors on internalization of human IgG by Caco-2 human intestinal epithelial cells, Life Sci.. 85 (23–26) (2009) 800–807.
[55] Z. Qian, et al., Early endosomal escape of a cyclic cell-penetrating peptide allows effective cytosolic cargo delivery, Biochemistry 53 (24) (2014) 4034–4046.
[56] F. Duchardt, et al., A comprehensive model for the cellular uptake of cationic cell-penetrating peptides, Traffic 8 (7) (2007) 848–866.
[57] J. Mueller, et al., Comparison of cellular uptake using 22 CPPs in 4 different cell lines, Bioconjug. Chem. 19 (12) (2008) 2363–2374.
[58] J.P. Richard, et al., Cell-penetrating peptides. A reevaluation of the mechanism of cellular uptake, J. Biol. Chem. 278 (1) (2003) 585–590.
[59] A.F.L. Schneider, et al., Cellular uptake of large biomolecules enabled by cell-surface-reactive cell-penetrating peptide additives, Nat. Chem. 13 (6) (2021) 530–539.
[60] L. Peraro, et al., Cell penetration profiling using the chloroalkane penetration assay, J. Am. Chem. Soc. 140 (36) (2018) 11360–11369.
[61] A. Peier, et al., NanoClick: a high throughput, target-agnostic peptide cell permeability assay, ACS Chem. Biol. 16 (2) (2021) 293–309.
[62] J.M. Holub, et al., Improved assays for determining the cytosolic access of peptides, proteins, and their mimetics, Biochemistry 52 (50) (2013) 9036–9046.
[63] D. Birch, et al., Fluorophore labeling of a cell-penetrating peptide induces differential effects on its cellular distribution and affects cell viability. Biochimica et Biophysica Acta (BBA) -, Biomembranes 1859 (12) (2017) 2483–2494.
[64] A.T. Jones, E.J. Sayers, Cell entry of cell penetrating peptides: tales of tails wagging dogs, J. Control. Release 161 (2) (2012) 582–591.
[65] S.F. Hedegaard, et al., Fluorophore labeling of a cell-penetrating peptide significantly alters the mode and degree of biomembrane interaction, Sci. Rep. 8 (1) (2018) 6327.
[66] X. Lian, et al., High efficiency and long-term intracellular activity of an enzymatic nanofactory based on metal-organic frameworks, Nat. Commun. 8 (1) (2017) 2075.